Inference-based time-resolved chaos analysis of brain models: application to focal epilepsy

Yun Zhao
Faculty of Information Technology
Monash University
Clayton, Australia
yun.zhao@monash.edu

David B. Grayden
Department of Biomedical Engineering
The University of Melbourne
Parkville, Australia
grayden@unimelb.edu.au

Mario Boley
Faculty of Information Technology
Monash University
Clayton, Australia
mario.boley@monash.edu

Yueyang Liu
Faculty of Information Technology
Monash University
Clayton, Australia
yueyang.liu@monash.edu

Philippa J. Karoly
Department of Biomedical Engineering
The University of Melbourne
Parkville, Australia
karoly.p@unimelb.edu.au

Mark J. Cook
St Vincent's Hospital
The University of Melbourne
Melbourne, Australia
markcook@unimelb.edu.au

Levin Kuhlmann
Faculty of Information Technology
Monash University
Clayton, Australia
levin.kuhlmann@monash.edu

***Abstract*—This paper introduces a new inference-based framework for time-resolved chaos analysis of brain models and demonstrates its application to focal epileptic seizures. The intermittent nature of epileptic seizures exhibits an unpredictable behavior that shares some characteristics with chaotic systems. Epilepsy research often uses concepts from chaos theory and nonlinear dynamics to better understand the mechanisms of seizure initiation, propagation, and termination. Traditional methods estimate the degree of chaos in brain dynamics directly from time series data. This provides neither an accurate estimate of the chaos nor insights into the key neurophysiological processes driving brain dynamics during epileptic seizures. Therefore, this study proposes a new method to calculate Lyapunov spectra by combining time series data with neurophysiological brain models and a specialised nonlinear Kalman filter. This study thereby provides insights into the temporal evolution of chaos in epileptogenic regions during epileptic seizures and identifies external inputs from adjacent and distant brain regions as major drivers of altered levels of chaoticity. This paper underscores the importance of fusion of neurophysiological computational models and clinical time series data in understanding the dynamic and chaotic aspects of epilepsy to develop more effective diagnostic and treatment strategies.**

***Index Terms*—Chaos analysis, brain modeling, electroencephalography, Kalman filters, epilepsy**

I. Introduction

Epilepsy is a complex neurological disorder characterized by the occurrence of spontaneous seizures affecting millions worldwide [1]. Mainstream research in epilepsy involves understanding the complex mechanisms by which epileptic seizures are generated, propagated, and terminated. Recent explorations into chaos theory, recognizing epilepsy as potentially chaotic behavior, have introduced innovative mathematical techniques for analyzing electroencephalographs (EEG) [2]–[6]. These nonlinear dynamics and chaos theory applications offer fresh insights into the epileptogenic process, opening new avenues for diagnosis and treatment.

The application of chaos analysis in epilepsy studies marks a pivotal advancement towards recognizing the disorder's dynamic complexities. This approach is grounded in the principle that epileptic seizures may arise from deterministic chaotic processes within the brain's neuronal networks [7]. By reconstructing phase space from time series data—such as EEG recordings—researchers have been able to perform sophisticated analyses, including Lyapunov exponents calculation, to quantify the degree of chaos and predict seizure events [8], [9]. Such methodologies have underscored the relevance of nonlinear dynamics in understanding epilepsy, offering insights into the unpredictable and seemingly random nature of seizures.

Integrating chaos analysis with computational models can further deepen our understanding of epilepsy. Computational models, ranging from simple neuronal circuits to complex neural networks, contain meaningful neurophysiological variables and have become powerful tools for dissecting the mechanisms driving epileptiform activity. However, the primary focus of computational epilepsy research has largely been on identifying epileptogenic zones [10], exploring seizure pathways [11], and predicting seizures [12], with less emphasis on chaos analysis.

Therefore, we propose a novel framework that combines clinical data with computational modeling to perform inference-based time-resolved chaos analysis in epilepsy stud-

ies. This approach can overcome limitations of traditional methods by enabling the identification of specific neurophysiological variables that play pivotal roles in the chaotic behavior observed during seizures. By pinpointing these critical variables, our framework aims to illuminate the core components driving epilepsy's dynamic instability. Overall, this innovative integration of chaos theory, computational modeling, and clinical data provides a promising avenue to revolutionize our understanding of seizure mechanisms, with the potential to develop targeted therapies that can modulate these key neurophysiological factors and improve outcomes for individuals affected by this challenging disease. Moreover, this methods could also be used to study other kinds of brain dynamics such as those associated with sleep, anaesthesia, awake resting or functional task-based states.

II. Methods

A. Methods Outline

We begin by describing the dataset used in this study to obtain data-driven results. Next the basic component, a single neural population model, of the larger multiple regions brain model is described. After this the next scale of the model is described, namely the Jansen-Rit neural mass model (NMM) which represents a local model of cerebral cortex underlying a single intracranial EEG (iEEG) channel that consists of multiple neural populations. We next describe how multiple NMMs are connected to form a multiple regions model of the brain network underlying the set of recorded iEEG channels. Using this multiple regions model to capture the dynamics of a large scale brain network, we then apply a combination of novel NMM-specific nonlinear Kalman filtering and linear regression methods to estimate the time-varying parameters of the model from multichannel iEEG. These parameter estimates then facilitate a time-varying chaoticity analysis that is scalable, model-based and data-driven.

B. Dataset

Intracranial EEG from 2 focal epilepsy individuals with drug-resistant epilepsy was used in this study [13]. The individuals were selected based on their experience of 2 to 12 disabling partial-onset seizures per month and had various epilepsy etiologies. Regarding data collection protocol, patients underwent a surgical procedure to implant the seizure advisory system. This system comprised two silicon implantable lead assemblies, each featuring eight platinum iridium contacts distributed across two electrode arrays designed to collect iEEG data from the epileptogenic regions (Fig 1a). The leads were tunneled down the neck and connected to a subclavicularly placed titanium-encased, hermetically sealed implantable telemetry unit. This unit sampled 16 channels of iEEGs (Fig 1b) at 400 Hz and wirelessly transmitted these data to an external device. The implantable components were designed for long-term use but could be removed using standard surgical techniques. Following implantation, the study entered a data collection phase. iEEGs were recorded for each subject for 2 years. An algorithm was applied to extract iEEG segments from 60 seconds before seizure onset to 10 seconds after seizure offset. Overall, subject 1 had 112 recorded seizures and subject 3 had 331 recorded seizures.

C. Single Population Model

In the exploration of neural population dynamics, the inception point is the characterization of the mean membrane potential, v_n, attributed to a neural ensemble. This potential is quantitatively synthesized as a cumulative effect of mean post-synaptic potentials, v_{mn}, where the indices n and m demarcate post-synaptic and pre-synaptic neural assemblies, respectively. The genesis of the post-synaptic potential is mathematically depicted through the convolution operation involving the input firing rate, $\phi_m(t)$, and the post-synaptic response kernel, yielding the following expression,

$$v_{mn}(t) = \alpha_{mn} \int_0^t h_{mn}(t-t')\phi_m(t')dt', \tag{1}$$

where α_{mn} represents a lumped connectivity parameter including aspects such as synaptic efficacy, connectivity density, and the peak firing rates of pre-synaptic cohorts. The synaptic response kernel, $h_{mn}(t)$, is a function parameterized by its temporal constant, τ_{mn}, and is given as,

$$h_{mn}(t) = \eta(t)\frac{t}{\tau_{mn}} \exp\left(-\frac{t}{\tau_{mn}}\right), \tag{2}$$

with $\eta(t)$ representing the Heaviside step function. Inputs to the neural population, denoted as ϕ_m, may originate from external stimuli (μ) or other neural populations within the system, processed through an activation function, $g(v_m)$, which is defined based on the nature of the input, external or internal. This is encapsulated by,

$$\phi_m = \begin{cases} \mu & \text{if } m \text{ indexes external inputs,} \\ g(v_m) & \text{if } m \text{ indexes internal inputs.} \end{cases} \tag{3}$$

where $g()$, mapping the pre-synaptic mean membrane potential to a mean firing rate, adopts a sigmoidal relationship to capture the firing rate limitation imposed by the neuronal refractory period. $g()$ is given by

$$g(v_m) = \frac{1}{2}\left(\text{erf}\left(\frac{v_{mn}-v_0}{\sigma}\right)+1\right), \tag{4}$$

where σ delineates the slope of the sigmoid, or equivalently, the variance of firing thresholds within the pre-synaptic population, assuming a Gaussian distribution of these thresholds, and v_0 symbolizes the mean firing threshold relative to the resting membrane potential.

The convolution in Equation (1) can be conveniently written as two coupled first-order ordinary differential equations (ODEs),

$$\frac{\mathrm{d}v_{mn}}{\mathrm{d}t} = z_{mn}, \quad \frac{\mathrm{d}z_{mn}}{\mathrm{d}t} = \alpha_{mn}g(v_m) - \frac{2}{\tau_{mn}}z_{mn} - \frac{1}{\tau_{mn}^2}v_{mn}. \tag{5}$$

In essence, this model depicts the transformation from a mean pre-synaptic firing rate to a post-synaptic potential, with critical parameters including synaptic time constants (τ_{mn}),

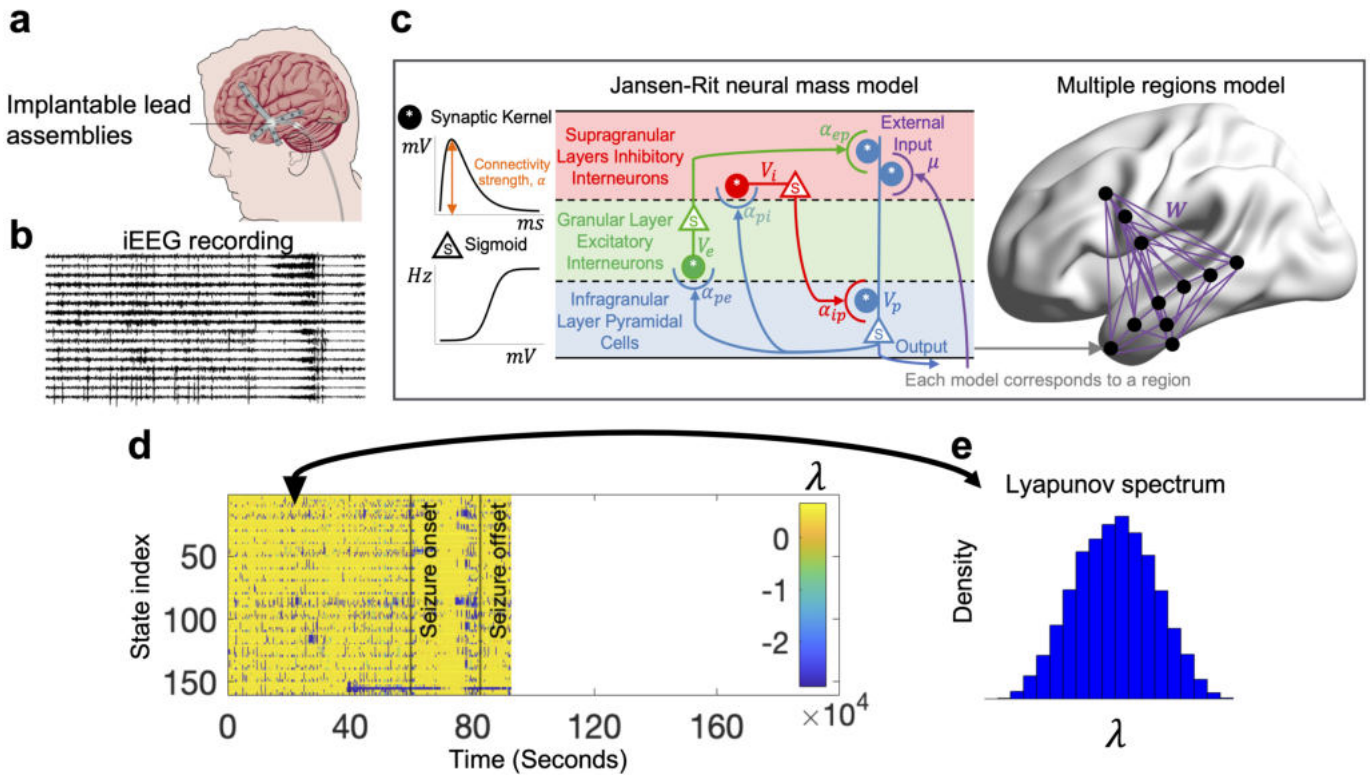

Fig. 1. a. 16-channel intracranial electrode arrays, indicated by the grey areas, were utilized for gathering intracranial electroencephalogram (iEEG) data from the cortical surface. b. Example of iEEG recording during a patient's seizure. c. Schematic of the modelling framework. c. Left: Jansen-Rit NMM. Three local neural populations are linked via synaptic kernels with connectivity strength α_{mn}. Right: the multiple regions model is composed of many NMMs interconnected, where each NMM represents a cortical region. $\mathbf{W}$ defines the inter-regional connection strength. d. The time-varying Lyapunov spectrum of the model during an example seizure is depicted. Each row in the diagram corresponds to the Lyapunov exponent associated with the states of the multiple regions model, while each column represents the Lyapunov spectrum at each time step. e. The Lyapunov spectrum of the model at a specific time step is illustrated.

connectivity constants (α_{mn}), mean firing thresholds (v_0), and threshold variances (σ). These parameters are vital for portraying specific interconnections among neural populations, such as pyramidal cells, excitatory and inhibitory interneurons.

D. Jansen-Rit neural mass model (NMM)

The architecture of a cortical region can be depicted through the integration of multiple neural populations, analogous to the structural organization within a cortical column. This is achieved by employing a configuration akin to the model expressed in Equation (5), wherein each synaptic linkage is represented by a duo of coupled first-order ODEs. The conceptual framework for this multi-population model draws inspiration from the works of Jansen and Rit [14] and has been elaborated in preceding studies [11], [15]–[18]. Jansen-Rit NMM is shown in Fig 1c. The model encompasses three distinct neural populations: excitatory (e), inhibitory (i), and pyramidal (p). The dynamics and interplay between these populations are central to the generation of iEEG signals, reflecting the synaptic currents primarily influenced by inputs to the pyramidal neurons.

The state of the model is encapsulated by the vector:

$$\mathbf{x} = [v_{ip}\ z_{ip}\ v_{pi}\ z_{pi}\ v_{pe}\ z_{pe}\ v_{ep}\ z_{ep}]^\top, \tag{6}$$

accompanied by a parameter vector that includes external inputs and all synaptic strengths:

$$\boldsymbol{\theta} = [\mu\ \alpha_{ip}\ \alpha_{pi}\ \alpha_{pe}\ \alpha_{ep}]^\top. \tag{7}$$

This model is augmented to include both the state and parameter vectors,

$$\boldsymbol{\xi} = [\boldsymbol{x}^\top \boldsymbol{\theta}^\top]^\top. \tag{8}$$

This leads to an augmented state-space representation that facilitates the inclusion of stochastic dynamics and uncertainty, essential for predictive modeling and parameter estimation through techniques such as Kalman filtering.

The augmented state-space model is delineated as follows:

$$\dot{\boldsymbol{\xi}} = \mathbf{A}\boldsymbol{\xi} + \mathbf{B}\boldsymbol{\xi} \odot g(\mathbf{C}\boldsymbol{\xi}), \tag{9}$$

where $\odot$ denotes element-wise multiplication, and matrices $\mathbf{A}$, $\mathbf{B}$, and $\mathbf{C}$ are defined in [16].

This model's discretization, necessary for computational simulations and Bayesian inference, incorporates an Gaussian white noise term, $\mathbf{w}_t$, to account for model uncertainty and external inputs. The discretized model with noise is given by,

$$\boldsymbol{\xi}_{t+1} = \mathbf{A}\xi_t + \mathbf{B}\xi_t \odot g(\mathbf{C}\xi_t) + \mathbf{w}_t. \tag{10}$$

The measurement model, essential for linking the model's output to observable iEEG data, is represented by:

$$y_t = \mathbf{H}\boldsymbol{\xi}_t + v_t, \tag{11}$$

with $\mathbf{H}$ being the observation matrix and v_t modeling measurement noise.

E. Multiple regions model

The model expands to incorporate multiple cortical areas by connecting the pyramidal population's output firing rate from one region to another's input through a synaptic response kernel as shown in Fig 1c [20]. This formulation uses the same second-order model defined in Equation (5) for the pyramidal population across all regions with inter-regional connections.

For the multi-region scenario, each cortical area is described using a NMM, extending the state vector to include states for post-synaptic potentials influenced by neuronal activities from other regions. The state vector for a given region, for example in a, is thus represented as

$$\mathbf{x}_a = [v_{ip}^a \; z_{ip}^a \; v_{pi}^a \; z_{pi}^a \; v_{pe}^a \; z_{pe}^a \; v_{ep}^a \; z_{ep}^a \; \mu^a \; u^a]^\top, \tag{12}$$

where μ represents the post-synaptic membrane potential induced by inter-regional firing rates, and u is the time derivative of μ. The dynamics within each region are governed by differential equations that take into account both the intrinsic properties of the region and its interactions with other regions. For instance, the dynamics for region a are described by

$$\begin{aligned}
\frac{\mathrm{d}v_{\mathrm{ip}}^a}{\mathrm{d}t} &= z_{\mathrm{ip}}^a & \frac{\mathrm{d}z_{\mathrm{ip}}^a}{\mathrm{d}t} &= \alpha_{\mathrm{ip}}^a g(v_{\mathrm{pi}}^a) - \frac{2}{\tau_{\mathrm{ip}}} z_{\mathrm{ip}}^a - \frac{1}{\tau_{\mathrm{ip}}^2} v_{\mathrm{ip}}^a \\
\frac{\mathrm{d}v_{\mathrm{pi}}^a}{\mathrm{d}t} &= z_{\mathrm{pi}}^a & \frac{\mathrm{d}z_{\mathrm{pi}}^a}{\mathrm{d}t} &= \alpha_{\mathrm{pi}}^a g(v_{\mathrm{ip}}^a + v_{\mathrm{ep}}^a + \mu^a) - \frac{2}{\tau_{\mathrm{pi}}} z_{\mathrm{pi}}^a - \frac{1}{\tau_{\mathrm{pi}}^2} v_{\mathrm{pi}}^a \\
\frac{\mathrm{d}v_{\mathrm{pe}}^a}{\mathrm{d}t} &= z_{\mathrm{pe}}^a & \frac{\mathrm{d}z_{\mathrm{pe}}^a}{\mathrm{d}t} &= \alpha_{\mathrm{pe}}^a g(v_{\mathrm{ip}}^a + v_{\mathrm{ep}}^a + \mu^a) - \frac{2}{\tau_{\mathrm{pe}}} z_{\mathrm{pe}}^a - \frac{1}{\tau_{\mathrm{pe}}^2} v_{\mathrm{pe}}^a \\
\frac{\mathrm{d}v_{\mathrm{ep}}^a}{\mathrm{d}t} &= z_{\mathrm{ep}}^a & \frac{\mathrm{d}z_{\mathrm{ep}}^a}{\mathrm{d}t} &= \alpha_{\mathrm{ep}}^a g(v_{\mathrm{pe}}^a) - \frac{2}{\tau_{\mathrm{ep}}} z_{\mathrm{ep}}^a - \frac{1}{\tau_{\mathrm{ep}}^2} v_{\mathrm{ep}}^a \\
\frac{\mathrm{d}\mu^a}{\mathrm{d}t} &= u^a & \frac{\mathrm{d}u^a}{\mathrm{d}t} &= \sum_{b=1}^{N} w_{ba} g(v_{\mathrm{ip}}^b + v_{\mathrm{ep}}^b + \mu^b) - \frac{2}{\tau_{\mathrm{d}}} u^a - \frac{1}{\tau_{\mathrm{d}}^2} \mu^a,
\end{aligned} \tag{13}$$

where b indicates a model in region b, w_{ba} represents the connectivity strength from b to a. Let $\mathbf{X}$ include all state variables of n_y regions $\mathbf{X} = [\mathbf{x}^1, \mathbf{x}^2, \ldots, \mathbf{x}^{n_y}]^\top$, the multiple regions model can then be described as a system of differential equations

$$\dot{\mathbf{X}} = f(\mathbf{X}) \tag{14}$$

where f is a map from $\mathbb{R}^{n_y \times 10}$ to $\mathbb{R}^{n_y \times 10}$. In this case $n_y = 16$ to model the 16 iEEG channels in the data.

F. Parameter estimation from data

To estimate $\boldsymbol{\xi}$ of each NMM in the multiple regions model, we treat each NMM in the network independent and apply our previously developed semi-analytical Kalman filter [16]. Briefly, the filter takes a single source time series (iEEG in this study) and estimates local NMM parameters $\boldsymbol{\xi}$ over time.

Since μ is the summation of post-synaptic membrane potentials induced by firing rate from other regions, μ in region a is

$$\mu^a(t) = \sum_{b=1}^{N} w_{ba} \int_0^t h_{ba}(t - t') g(v_p^b(t')) \mathrm{d}t', \tag{15}$$

where v_p^b denotes the membrane potential of pyramidal population in region b. The inter-regional connection strength w_{ba} is estimated by multivariate linear regression. The reason we do not use Kalman filters to estimate the inter-regional connectivity parameters is that we want to keep the method computationally efficient.

The multivariate regression model relates more than one predictor and more than one response. Let $\mathbf{Z}$ be an $n \times N$ matrix where each column is a μ estimate time series, $\mathbf{F}$ be an $n \times N$ matrix where each column is a time series of the convolution of the post-synaptic kernel with v_p estimates. Let $\mathbf{W}$ be an $N \times N$ matrix of coefficients w_{ba}, and $\mathbf{E}$ be an $n \times N$ Gaussian white noise. The multivariate regression model is defined by

$$\mathbf{Z} = \mathbf{F}\mathbf{W} + \mathbf{E} \tag{16}$$

where the maximum likelihood estimation and unbiased estimator for $\mathbf{W}$ is given as $\hat{\mathbf{W}} = (\mathbf{F}^\top \mathbf{F})^{-1} \mathbf{F}^\top \mathbf{Z}$.

G. Chaos analysis

The exploration of dynamical stability in models encompassing multiple cortical regions employs Lyapunov exponents to assess the divergence or convergence of closely initiated trajectories within the system's phase space. This divergence, indicative of chaotic dynamics, is quantitatively measured by Lyapunov exponents, which ascertain the exponential rate at which trajectories separate or merge over time. For the multi-regional model in Equation (14), consider a perturbation $\delta\mathbf{X}(t)$ to the trajectory $\mathbf{X}(t)$. The rate of change of this perturbation is governed by the Jacobian $\mathbf{J}(\mathbf{X}(t))$ of the vector field evaluated at the trajectory,

$$\delta\dot{\mathbf{X}}(t) = \mathbf{J}(\mathbf{X}(t))\delta\mathbf{X}(t). \tag{17}$$

The Lyapunov exponent, λ, is defined in terms of the exponential rate of growth of the perturbation over time,

$$\lambda = \lim_{t \to \infty} \frac{1}{t} \ln|\delta\mathbf{X}(t)|, \tag{18}$$

given an initial perturbation $\delta\mathbf{X}(0)$. It is typical to use the maximal Lyapunov exponent ($L_{\max}$) as a measure for the predictability for a system.

As the multiple regions model is nonlinear and high-dimensional, the Lyapunov spectrum is obtained through simulations of the model using the time-varying parameter estimates obtained in the previous section. The process involves numerically integrating the system's equations to track how small perturbations to initial conditions evolve over time. First, a set of initial conditions is chosen. Alongside the main trajectory, small deviations are introduced to these initial conditions to create a bundle of nearby trajectories. As the system evolves, numerical integration methods are applied to

simulate both the primary and perturbed trajectories. Periodically, the divergence between these trajectories is measured and normalized through orthonormalization procedures like the Gram-Schmidt process. This step prevents the perturbations from aligning along the direction of maximum expansion and maintains numerical stability. The exponential rate at which these perturbations grow or shrink, averaged over a sufficiently long time, yields the Lyapunov exponents. The spectrum of these exponents, sorted from largest to smallest, provides insight into the system's dynamics, revealing the presence and intensity of chaos. Positive Lyapunov exponents indicate sensitive dependence on initial conditions—a hallmark of chaotic behavior—whereas negative values suggest convergence to stable states or cycles.

III. Results

A. Cortical chaos analysis during seizures

We tracked the chaoticity of the multiple regions model over time during seizures by splitting the 16-channel iEEG time series into short (0.1 second), consecutive, non-overlapping windows. In each window, we inferred the model parameter $\mathbf{X}$, and calculated Lyapunov spectrum of the model with parameter estimates. Consequently, the time-varying Lyapunov spectrum (TLS) of the model was obtained by combining results from each time window. Fig 1d shows the TLS for an example seizure recording. Fig 1e shows a Lyapunov spectrum of the model at a particular time step. L_{max} was identified from the Lyapunov spectrum at each time step, resulting in a time-varying L_{max} to indicate the dynamic chaotic nature of the epileptogenic regions during a seizure. Such that, we obtained the time-varying L_{max} for all seizure recordings for subject 1 and 3 in this study, as shown in Fig 2a and c. Overall, L_{max} remained positive during epileptic seizures, indicating that the epileptogenic region was always in a chaotic state from preseizure to seizure and finally to postseizure time periods. But the level of chaoticity varied significantly at different phases. For both short and long seizures, we identified a general trajectory of chaos in epileptogenic zones. Initially, there was a reduction in chaos during the preseizure phase (potentially due to equilibration of the parameter estimation filter/boundary conditions), followed by a pronounced decline immediately post-epilepsy onset, reaching a nadir. Subsequently, chaos exhibited a resurgence, stabilizing at or surpassing the chaos levels at 60 seconds prior to the seizure onset.

To highlight the chaoticity change across seizures, we computed the mean of L_{max} and its 95% confidence interval, as shown in Fig 2b and d respectively for subject 1 and 3. Since the length of each epilepsy recording is different, Fig 2b and d only show L_{max} from the start to the time point where the shortest seizure ended. Some findings can be drawn from Fig 2b and d. First, L_{max} started to decrease before the onset, with a large decrease at the beginning, and then the rate of decrease gradually slows down but kept decreasing during this period (As noted above the initial large decrease may be due to boundary conditions). Second, in the preseizure period the confidence intervals for the mean of L_{max} around the start of the recording were narrower than that in the following time period. This indicates that across all seizures the chaoticity of the epileptogenic regions followed a similar pattern in the early stages of the preseizure period, and became different as the onset of epilepsy is approaching. Third, for subjects 1 and 3, L_{max} dropped sharply within 10 and 5 seconds, respectively, after the onset of seizure. Then L_{max} quickly rose to a level close to 60 seconds before the onset of seizure.

B. Dynamic chaos driver during seizures

We computed the temporal evolution of the Lyapunov spectrum for each seizure based on the multiple regions model and parameter estimates inferred from iEEG data. Theoretically, each Lyapunov exponent in the spectrum corresponds to a model state. This facilitates the identification of a critical model state associated with L_{max}. Since the cerebral cortex exhibits chaotic behaviour during epileptic seizures, determining which model state contributes significantly to the disorganized behavior of the system helps identify the neurophysiological mechanisms driving cortical chaos. For this, we determined the model state corresponding to L_{max} in each time window (exemplified in Fig 3a and b). Given that the multiple regions model consists of interconnected NMMs that have the same architecture and contain the same types of neurophysiological model states, we then determined the types of neurophysiological states associated with L_{max} in each time window (exemplified in Fig 3c). We finally can identify the most critical model state that always associates with L_{max} during the whole seizure recording.

Figure 3d illustrates that, regarding subject 1, the time derivative of the external input, denoted as u, acted as the primary driver of chaotic dynamics within epileptogenic zones in 37% of the seizures, whereas z_{ep}, representing the time derivative of the post-synaptic membrane potential from excitatory to pyramidal neuronal populations, served as the primary chaos driver in 36% of seizures. For subject 3, the external input μ was identified as the predominant driver of chaotic activity in the epileptogenic regions in over 50% of seizures, with u being the main chaotic driver in 40% of the seizures.

IV. Discussion

This study provides a novel framework for analyzing the chaoticity over time from time series data in selected brain regions or even the entire cerebral cortex during epileptic seizures or other brain conditions. Specifically, a multiple regions model is used to model the dynamics and neurophysiological processes in selected regions. The model consists of biophysically reasonable Jansen-Rit NMMs, contains meaningful neurophysiological variables, and has demonstrated its ability to model a variety of brain dynamics [15]–[17], [20]–[22]. Model parameters are then inferred from the observed time series data. Finally, the Lyapunov exponents are calculated based on the dynamics of the model. As oppose to this model-driven method, "Wolf algorithm", named after

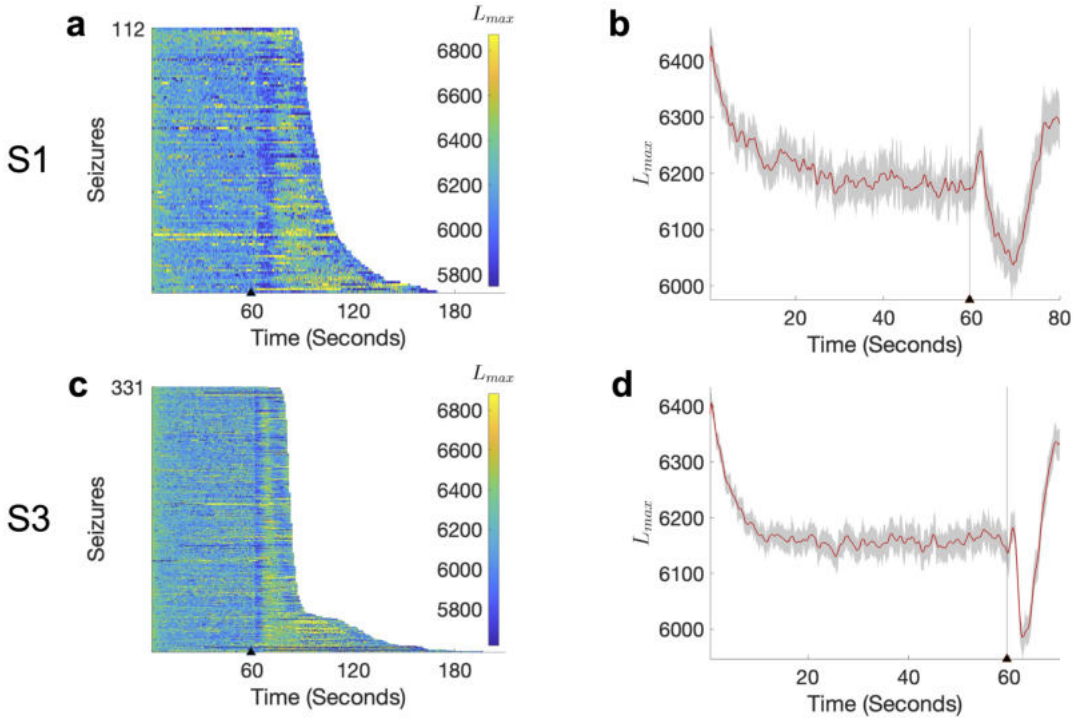

Fig. 2. a, c. The time-varying maximum Lyapunov exponent (L_{max}) of the multiple regions model for all seizure recordings from subject 1 and 3 is displayed, with rows sorted based on the length of the recording. Each row illustrates the time-varying L_{max} in each seizure. Black triangles on the x-axis mark the onset of seizures. b, d. The mean and 95% confidence interval of L_{max} are shown for the period from preseizure to onset of seizure across all seizures from subject 1 and 3. Black triangles on the x-axis mark the onset of seizures.

Alan Wolf et al., estimates the Lyapunov spectrum from the reconstructed phase space from time series data [8], [23], [24], [26]. The Wolf algorithm is a data-driven approach that does not require any priori knowledge about the system's mathematical model. It is particularly useful when the underlying equations of the system are unknown or too complex to be modeled accurately. Our method offers several advantages over the Wolf algorithm. 1) **Accuracy**: our method can offer more precise calculations of Lyapunov exponents, as it directly incorporates the system's mathematical structure. This can be particularly advantageous in theoretical studies or simulations where the exact equations governing the system's behavior are known. 2) **Identification of Chaotic Driver**: our method allows identifying the key neurophysiological variables that drives the chaotic behaviour of the brain dynamics, which helps understand the underlying neurophysiological processes of brain conditions and suggest appropriate intervening or target treatment for brain disorders. 3) **Flexibility in Analysis**: our method can explore the effects of parameter changes on system stability and perform sensitivity analyses. This is valuable in identifying conditions that may lead to chaotic behaviour. We applied this framework to explore the chaotic nature of brain dynamics during focal epileptic seizures and provide insights into the multifaceted and elusive mechanisms of epileptic seizures.

The analysis of cortical chaos during seizures provides insights into the dynamics of epileptogenic regions. We found the following. 1) **Persistent Chaos Throughout Seizure Phases**: the observation that the epileptogenic regions consistently exhibit chaotic behavior during seizures underscores the inherently unpredictable nature of seizure dynamics. 2) **Reversible Reduction of Chaos**: epileptic seizures are accompanied by sudden and large increases in the predictability of brain states, suggesting that seizures are events that are initially difficult to halt by the brain itself once they have begun. Similar to the traditional perception with data-driven methods, as the seizure progresses, L_{max} gradually rises and finally exceeds that of the preseizure state [2], [3]. 3) **Consistency in Early Preseizure Phase**: the narrower confidence intervals for L_{max} during the early stages of the preseizure period suggest a potentially predictable change in brain dynamics leading up to a seizure, which could be relevant to the fixed seizure genesis mechanism of an individual.

We present an investigation of the drivers behind chaotic dynamics within epileptogenic regions during seizures. Specifically we found the following. 1) **Diverse Mechanisms of Chaos Modulation**: the chaotic behavior observed in epileptogenic zones can be driven through different mechanisms, as evidenced by the significant roles played by the external input (u and μ) and the time derivative of the post-synaptic membrane potential from excitatory to pyramidal population (z_{ep}). 2) **Variability Among Subjects**: the fact that different chaos drivers have been identified as primary in different subjects underscores the individual variability in the pathological

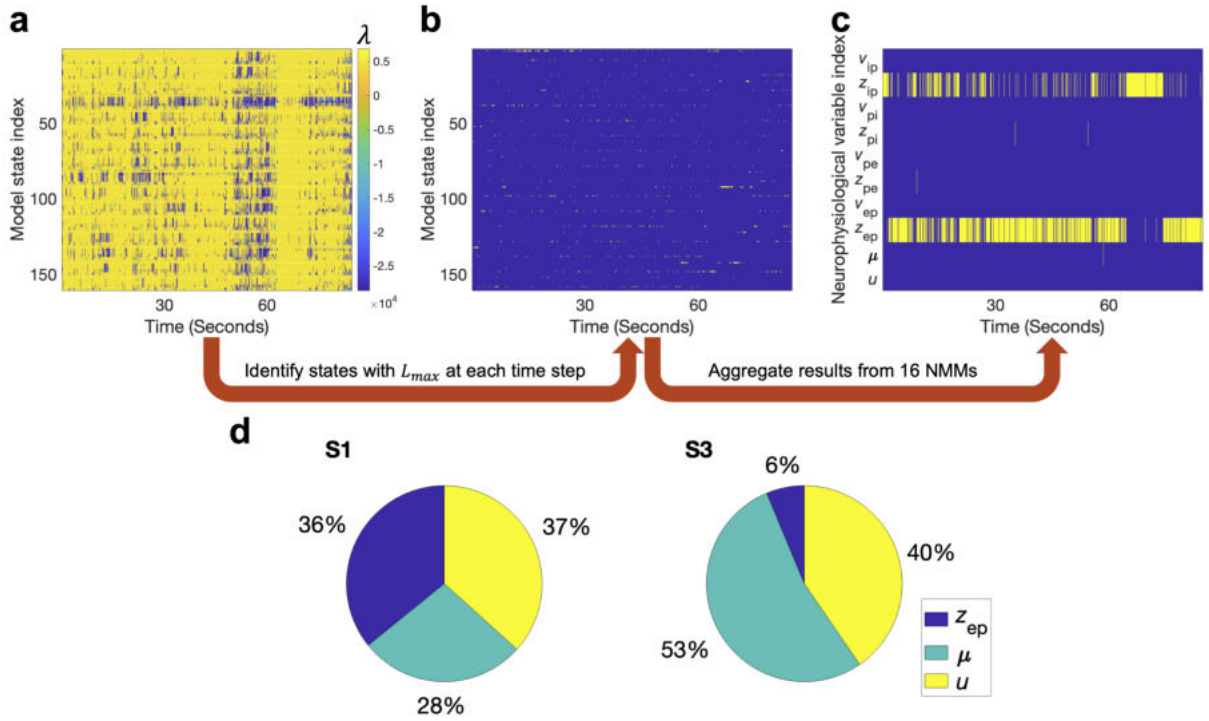

Fig. 3. a. The time-varying Lyapunov spectrum of the model for an example seizure. b. The yellow point in each column indicates the model state associated with L_{max} at each time step. c. The yellow point in each column indicates the neurophysiological variable type associated with L_{max} at each time step. The chaotic driver refers to the variable with L_{max} for the majority of the time. d. The proportion of each neurophysiological variable type as the chaos driver across all epilepsy recordings for subject 1 and 3. Neurophysiological variables accounting for less than 1% are not displayed.

mechanisms underlying seizures. This variability emphasizes the importance of personalized approaches in understanding and potentially treating epilepsy. 3) **Predominance of External Inputs in Driving Chaos**: the finding that external inputs are significant drivers of chaos in a substantial proportion of seizures highlights the critical role of external or systemic factors in influencing the epileptogenic regions' dynamics. It suggests that interventions aimed at modulating these inputs might be effective in controlling or intervening with the chaotic behavior associated with seizures. 4) **Implications for Treatment Strategies**: treatments that stabilize or perturb the external input (relevant to inter-regional connectivity) or its temporal derivatives might prove effective in reducing the occurrence or severity of seizures in some patients.

Here we have presented a scalable model-based data-driven method for chaoticity analysis in large scale brain systems that also offers neurophysiological interpretability. The framework is general enough to work for arbitrary kinds of NMMs. As such it should provide a basis for chaoticity analysis of brain functions in both health and disease.

Ethical approval statement

Use of this data in this paper is approved by Human Research Ethics Committee, St Vincent's Hospital, Melbourne–approval LRR145/13.

Acknowledgment

This work is supported by grants from the Australian Research Council (DP210100045) and Monash University. We thank MASSIVE (https://www.massive.org.au) for computational resources.

References

[1] Beghi, Ettore. "The epidemiology of epilepsy." Neuroepidemiology 54.2 (2020): 185-191.
[2] Iasemidis, Leonidas D., and J. Chris Sackellares. "REVIEW: Chaos Theory and Epilepsy." The Neuroscientist 2.2 (1996): 118-126.
[3] Sackellares, J. Chris, et al. "Epilepsy–when chaos fails." Chaos in Brain?. 2000. 112-133.
[4] Adeli, Hojjat, Samanwoy Ghosh-Dastidar, and Nahid Dadmehr. "A wavelet-chaos methodology for analysis of EEGs and EEG subbands to detect seizure and epilepsy." IEEE Transactions on Biomedical Engineering 54.2 (2007): 205-211.
[5] Panahi, Shirin, et al. "A new chaotic network model for epilepsy." Applied Mathematics and Computation 346 (2019): 395-407.
[6] Fei, Keling, et al. "Chaos feature study in fractional Fourier domain for preictal prediction of epileptic seizure." Neurocomputing 249 (2017): 290-298.
[7] Sohanian Haghighi, H., and Amir Hossein Davaie Markazi. "A new description of epileptic seizures based on dynamic analysis of a thalamocortical model." Scientific Reports 7.1 (2017): 13615.
[8] Wolf, Alan, et al. "Determining Lyapunov exponents from a time series." Physica D: nonlinear phenomena 16.3 (1985): 285-317.
[9] Iasemidis, Leonidas D., et al. "Phase space topography and the Lyapunov exponent of electrocorticograms in partial seizures." Brain topography 2 (1990): 187-201.
[10] Jehi, Lara. "The epileptogenic zone: concept and definition." Epilepsy currents 18.1 (2018): 12-16.
[11] Karoly, Philippa J., et al. "Seizure pathways: A model-based investigation." PLoS computational biology 14.10 (2018): e1006403.

[12] Kuhlmann, Levin, et al. "Seizure prediction—ready for a new era." Nature Reviews Neurology 14.10 (2018): 618-630.
[13] Cook, Mark J., et al. "Prediction of seizure likelihood with a long-term, implanted seizure advisory system in patients with drug-resistant epilepsy: a first-in-man study." The Lancet Neurology 12.6 (2013): 563-571.
[14] Jansen, Ben H., and Vincent G. Rit. "Electroencephalogram and visual evoked potential generation in a mathematical model of coupled cortical columns." Biological cybernetics 73.4 (1995): 357-366.
[15] Kuhlmann, Levin, et al. "Neural mass model-based tracking of anesthetic brain states." NeuroImage 133 (2016): 438-456.
[16] Zhao, Yun, et al. "Space-time resolved inference-based neurophysiological process imaging: Application to resting-state alpha rhythm." NeuroImage 263 (2022): 119592.
[17] David, Olivier, and Karl J. Friston. "A neural mass model for MEG/EEG:: coupling and neuronal dynamics." NeuroImage 20.3 (2003): 1743-1755.
[18] Freestone, Dean R., et al. "Estimation of effective connectivity via data-driven neural modeling." Frontiers in neuroscience (2014): 383.
[19] Simon, Dan. Optimal state estimation: Kalman, H infinity, and nonlinear approaches. John Wiley & Sons, 2006.
[20] Zhao, Yun, et al. "Inference-based time-resolved stability analysis of nonlinear whole-cortex modeling: application to Xenon anaesthesia." 2023 45th Annual International Conference of the IEEE Engineering in Medicine & Biology Society (EMBC). IEEE, 2023.
[21] Zhao, Yun, et al. "Improved Neurophysiological Process Imaging Through Optimization of Kalman Filter Initial Conditions." International Journal of Neural Systems 33.05 (2023): 2350024.
[22] Moran, Rosalyn, Dimitris A. Pinotsis, and Karl Friston. "Neural masses and fields in dynamic causal modeling." Frontiers in computational neuroscience 7 (2013): 57.
[23] Wolf, A. "Quantifying chaos with Lyapunov." Chaos (1986): 273.
[24] Kutepov, Ilya E., et al. "EEG analysis in patients with schizophrenia based on Lyapunov exponents." Informatics in medicine unlocked 18 (2020): 100289.
[25] Pechuk, Vasiliy D., Tatyana S. Krasnopolskaya, and Evgeniy D. Pechuk. "Maximum lyapunov exponent calculation." Chaotic Modeling and Simulation International Conference. Cham: Springer International Publishing, 2021.
[26] Grond, Florian, et al. "A robust, locally interpretable algorithm for Lyapunov exponents." Chaos, Solitons & Fractals 16.5 (2003): 841-852.